Experimental Investigation of Supersonic Flow Past Double-Wedge Configurations

John J. Bertin* and John C. Hinkle†
The University of Texas at Austin, Austin, Texas

Viscous-inviscid interactions characteristic of those which occur when the fuselage-generated shock wave interacts with the wing-generated shock wave of a shuttle orbiter were studied experimentally. Surface-pressure measurements and schlieren photographs were obtained to define the flowfield generated when a Mach 4.97 stream encounters a double-wedge configuration. The deflection angles for the two wedge surfaces were such that the shock interaction pattern was either a Type-V pattern or a Type-VI pattern, as defined by Edney. The correlation between the present data and the theoretical solution for the Type-VI solution is satisfactory. The correlation between the measured Type-V shock-interaction pattern and the theoretical solution is satisfactory up to the interaction region. Downstream of the interaction the Type-V data depend primarily on the shape of the leading-edge shock wave.

Nomenclature

L = streamwise length of the second wedge
p = static pressure
s = streamwise distance from the leading edge (for each plate)
y = distance from the plane of symmetry
δ = initial turning angle (see Fig. 1)
Λ = sweep angle (see Fig. 1)

Introduction

THE flowfield perturbation which results when the fuselage-generated shock wave interacts with the wing-generated shock wave is an important factor in the design of the shuttle entry configuration. Because of the complexity of the viscous-inviscid interaction phenomena, many experimental investigations of the locally perturbed flowfields use models consisting of elementary configurations. Using data from an experimental program which employed elementary configurations, Edney[1] defined the flow phenomena which characterize the various types of shock-interaction patterns. Hains and Keyes[2] have categorized the shock-interaction patterns obtained for a variety of space shuttle configurations in terms of the flow models of Edney. Bertin et al.,[3] examined surface-pressure and heat-transfer-rate data for a variety of shuttle orbiter configurations over an angle-of-attack range from 0°-60°. The correlations for these three-dimensional flows indicated that the "type" of shock-interaction pattern was dominated by the effective sweep angle of the leading edge. For the relatively low sweep angles of the straight-wing orbiters, the interaction between the bow-generated shock wave and the wing-generated shock wave exhibited the characteristics of a Type-V shock-interaction pattern. For delta-wing orbiters, the shock-shock interaction exhibited the characteristics of a Type-VI pattern for all angles of attack.

The data discussed were obtained in facilities where real gas effects would not be expected to significantly alter the shock-interaction phenomena. By comparing data from facilities using helium, air, nitrogen, and tetrafluoromethane as the test gases, Hunt and Creel[4] studied the effect of shock-density ratio on the body-shock-wing-shock interaction. The effect of the shock-density ratio, or equivalently the specific heat ratio (gamma), was found to be more significant on the Type-V pattern than on the Type-VI pattern. Numerical solutions[5] of two-dimensional shock-interaction flowfields indicated that, although the use of an effective gamma did not adequately represent real-gas effects, the theoretical Type-VI solution was significantly altered by inclusion of the actual thermodynamic properties of air. The major real-gas effect is that the minimum sweep angle for which a given pattern can exist is much lower when the real-gas effects are included.

Using the numerical codes described in Ref. 5, both the Type-V and the Type-VI shock-interaction patterns were found to exist theoretically for a given geometry subject to a given flow condition. In the Type-V shock-interaction pattern, a shock wave impinges on the wing leading-edge; while in the Type-VI pattern, an expansion wave impinges on the wing. Thus, it is important to establish experimentally which, if either, pattern dominates in the region of flow conditions where either pattern exists theoretically. The present investigation was undertaken to determine: 1) criteria governing the conditions for which a particular pattern exists; and 2) features of the viscous:inviscid interaction needed to improve the flowfield models for the theoretical analysis. Schlieren

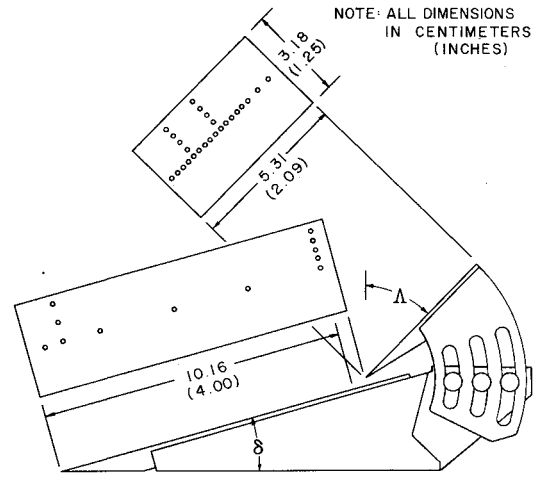

Fig. 1 Sketch of the double-wedge model.

Received August 5, 1974; revision received December 4, 1974. This work was supported by the Johnson Space Center, NASA Contract NAS9-13680.

Index categories: Jets, Wakes, and Viscid-Inviscid Flow Interactions; Supersonic and Hypersonic Flow.

*Associate Professor, Department of Aerospace Engineering and Engineering Mechanics. Member AIAA.

†Research Assistant, Department of Aerospace Engineering and Engineering Mechanics.

photographs, oil flow patterns, and surface pressure measurements were obtained when a double-wedge configuration was exposed to a supersonic stream. The nominal flow conditions were a freestream Mach number of 4.97 with a freestream Reynolds number of 0.634×10^6 per cm (19.3×10^6/ft). The geometric variables of the program were the deflection angles for the 2 wedge surfaces.

Experimental Program

Facility

The tests were conducted in the University of Texas Supersonic Wind Tunnel (UT SWT). The facility is a two-dimensional, blow-down-type wind tunnel, using air as the test gas. The nominal dimensions of the test section are width 15.3 cm (6.0 in.) by height 17.8 cm (7.0 in.). The test section diverges slightly along its length to accommodate boundary-layer growth.

Test Conditions

The freestream Mach number for the tests was 4.97 ± 0.02. The stagnation pressure was 2.16×10^6 N/m^2 (309 psia) with a maximum fluctuation during a run of $\pm 1.378 \times 10^4$N/m^2 (±2 psia). The stagnation temperature range was 294K (530° R) to 299K (539°R). As a result, the nominal freestream Reynolds number was 0.634×10^6/cm (19.3×10^6/ft).

Models

A sketch of the double-wedge model used during the test program is shown in Fig. 1. Two different support bases were used so that the effect of the initial wedge angle could be studied. For one model the initial wedge angle (δ) was 5°, for the other it was 15°. The second wedge was intended to represent ("two-dimensionally") the leading edge of a wing. For each model, the wedge angle was varied through a range of sweep angles from 34°-50°. The dimensions of the model were restricted because of blockage considerations.

The plate which constituted the (variable-sweep) second wedge was 5.31 cm (2.09 in.) in length. Both plates were 3.18 cm (1.25 in.) in width. During the tests, a constant gap of 0.24 cm (0.092 in.) was maintained between the 2 wedges to allow for boundary-layer bleed off and, thus, eliminate the possibility of separation in the corner intersection of the 2 wedges.

A total of 37 static pressure orifices were located on the surface of each model: 12 on the first wedge and 25 on the second wedge. The pressure taps were located primarily on the center line of the 2 surfaces. Because of the restricted model size, three-dimensional effects were expected. Therefore, pressure taps were located transversely at 2 stations on each of the 2 plates. Two photographs of a typical test setup are presented in Fig. 2. The photographs show the 2 basic models used in the program, i.e., for one model the initial wedge angle was 5° and for the second model it was 15°. The models were mounted in the test-section using a floor-mounted support system. Leads from the static pressure orifices were taken out of the tunnel aft of the model to a mercury-filled manometer board from which the surface pressure measurements were obtained. The maximum visual error in reading the manometer boards corresponds to a pressure error of ±70 N/m^2 (±0.01 psi).

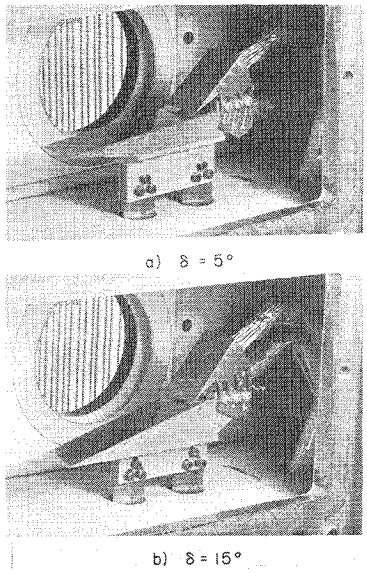

a) δ = 5°

b) δ = 15°

Fig. 2 Photographs of the two basic models in the University of Texas Supersonic Wind Tunnel.

Discussion of Results

Limits for a Particular Shock-Interaction Pattern

Characteristics of the shock-interaction patterns for a double-wedge configuration depend on the deflection angle of the first wedge, the sweep angle of the second wedge (or "simulated" wing) of the model, the freestream flow condition, and the gas property model. The minimum sweep angle for which a Type-V pattern is possible is that for which the flow in the shock-layer adjacent to the first wedge can be turned parallel to the second wedge (inboard of the intersection region) by a linear, oblique shock wave. The Type-VI shock-interaction characteristics no longer exist when the sweep angle becomes so small that the required outboard shock-layer flow (i.e., outboard of the intersection region) cannot be generated by a single weak shock wave.

Schlieren photographs and static wall-pressure distributions along the second wedge were used to determine which pattern existed for a given geometry. The minimum sweep angle for which a particular interaction pattern was observed experimentally is presented in Table 1 and in Fig. 3. The experimentally determined values are compared with the theoretical lower limits using the criteria defined in the previous paragraph. The theoretical values of Table 1 represent the values of Ref. 6 for a wedge and for a cone. The measured values are in approximate agreement with the values for the two-dimensional, wedge flow. Note also that, in the region where either the Type-V pattern or the Type-VI pattern are theoretically possible,[5] the weaker, Type-VI pattern is observed experimentally.

For $\delta = 15°$, the sweep angles at which a significant change occurred in the flowfield could be readily defined using the static wall-pressure distributions and the schlieren photographs. For $\delta = 5°$, a static wall-pressure distribution characteristic of the Type-V pattern was not obtained for the sweep angles tested (see Fig. 3a). Furthermore, the pressure distributions obtained for sweep angles of 46°, or less, were significantly different than the Type-VI distributions obtained at the greater sweep angles. Thus, the lower limit of the Type-

Table 1 The smallest sweep angle for which a given shock-interaction pattern occurs

a) $\delta = 5°$

Shock-interaction pattern	Measured Λ_{min}	Wedge theory Λ_{min}	Cone theory Λ_{min}
Type VI	48°	49.0°	35.5°
Type V	47° (approx)	45.0°	31.2°

b) $\delta = 15°$

Shock-interaction pattern	Measured Λ_{min}	Wedge theory Λ_{min}	Cone theory Λ_{min}
Type VI	47°	49.0°	35.5°
Type V	36°	37.7°	24.6°

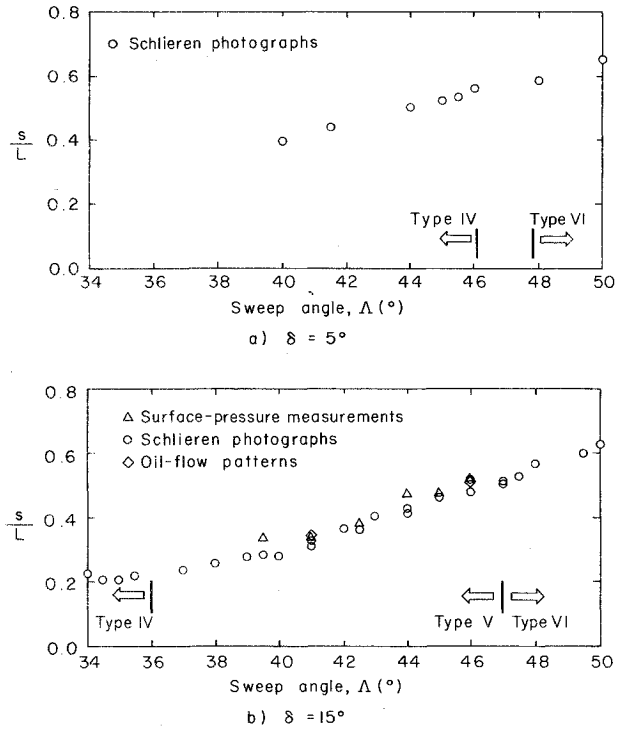

Fig. 3 Location of the interaction perturbed region on the second wedge as a function of sweep angle. a) $\delta = 5°$; b) $\delta = 15°$.

V pattern is less than 48° (the smallest angle for which a Type VI pattern was observed) but greater than 46°. That the Type-V pattern should exist only over a brief range of sweep angles when $\delta = 5°$ is not surprising. Because the "bow" shock wave is weak, the flow in the shock layer adjacent to the first wedge is only slightly different from the freestream flow. Thus, the minimum deflection angle for which it is possible to have a linear, oblique shock wave turn the flow parallel to the second wedge for the root region is essentially the same as that for the outboard region.

For a Type-VI shock-interaction pattern, the location of the interaction-perturbed region is uniquely defined by the computer code described in Ref. 7. However, for a Type-V shock-interaction pattern, the numerical code of Ref. 8 does not uniquely define the interaction-perturbed region. Therefore, one must input certain characteristic lengths so that the interaction geometry for the Type-V interaction can be computed by the program.

Schlieren photographs, surface-pressure distributions, and oil-flow patterns have been used to determine that region of the second wedge, i.e., the simulated wing leading edge, which is affected by the shock-interaction. The experimentally determined locations of the interaction perturbed region, which are presented in Fig. 3, represent the upstream end of the perturbed region. The location of the interaction is independent of the technique used. The largest "discrepancies" appear in the locations determined using the pressure data. This is understandable since the pressures were measured at a finite number of specific locations.

Over the range of sweep angle tested, the location of the perturbed region moves inboard as the sweep angle decreases. It is interesting to note that the curve is continuous even as the interaction pattern changes character, e.g., from Type VI to Type V. Thus, as the wing leading-edge shock increases in strength (with a corresponding increase in the downstream pressure) so that the wave impinging on the surface goes from an expansion wave (Type-VI) to a compression wave (Type-V), the impingement location does not change suddenly. The fact that the experimentally-determined interaction location is a "well-behaved" function of sweep will be useful to a numerical solution which requires empirical inputs.

The Type-V Results

As noted in the section discussing the limiting mechanisms, a Type-V pattern occurs when the sweep angle becomes so small that the required outboard flow cannot be generated by a single, weak shock wave. For $\delta = 15°$, data characteristic of the Type-V interaction were obtained for sweep angles from 37°-46°. Definite changes in the Type-V flowfield occur as the sweep angle is changes. Based on the theoretical solutions of Ref. 8, it is evident that, as the sweep angle is decreased, the impinging shock wave becomes more normal causing the downstream Mach number to go from supersonic values to subsonic values. At relatively high sweep angles, the flow downstream of the impinging shock is still supersonic and a reflected shock wave is generated. For an intermediate Type-V sweep-angle, the impinging shock has become so strong that the downstream flow is subsonic. Thus, the theoretical solution yields a Type-V flow model with a Mach reflection.

The experimentally observed shock structure for an intermediate Type-V sweep angle, i.e., $\Lambda = 41°$, is compared in Fig. 4 with the theoretical solution. For a given test condition, the shock-wave angles are uniquely determined by the numerical code described in Ref. 8. The computed angle of the wing-root shock wave, i.e., the shock wave dividing Region 2 from Region 3, is 55° (with respect to the surface of the initial wedge) while the experimental value is 52°. The difference between the experimental and the theoretical values is attributed to the fact that the actual Mach number in Region 2 just upstream of the "wing-root" shock is greater than the theoretical value. This conclusion is based on the static pressure measurements for the first wedge, which indicate that the flow accelerates along the length of the plate. The pressure near the leading edge is slightly above the theoretical value for a 15° deflection of the freestream flow, while the pressure measured near the intersection with the second wedge is slightly below the theoretical value. Thus, just upstream of the wing-root shock, the local Mach number is greater than the theoretical value.

Because the flowfield contains both subsonic and supersonic regions, the lengths of the shock-wave elements are not determined by the current numerical code. Therefore, to compute the geometry of the shock structure, one must input either the length of the shock wave which divides Region 2 from Region 5 or the surface length of Region 3. For the computed geometry presented in Fig. 4, the length of the shock wave dividing Region 2 from Region 5 was assumed to be equal to the experimentally observed value.

The theoretical values for the angles for the various shock-wave elements correlate well with the experimentally determined values. There is also good agreement between the theoretical and the experimental values for the flow direction in Region 4 and in Region 5. This agreement can be seen by noting the similarity between the calculated and the observed shear layer dividing Region 4 from Region 5. Thus, the difference between the calculated and the measured values for the wing-root shock wave contributes significantly to the dif-

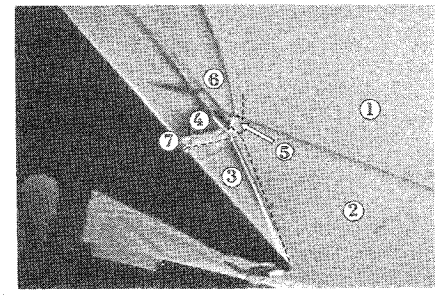

Fig. 4 Comparison of the theoretical flowfield using the Type-V code of Ref. 8 with the schlieren photograph: $M_\infty = 4.97$, $\delta = 15°$; $\Lambda = 41°$. Theoretical Mach numbers: Region 1: 4.97, Region 2: 3.49, Region 3: 1.35, Region 4: 1.06, Region 5: 0.57, Region 6: 0.42, Region 7: 0.76.

ferences between the flowfield computed by the theoretical code and that portrayed in the schlieren photograph. The correlation, however, is considered good.

The theoretical Mach number of 0.42 which is tabulated in Fig. 4 for Region 6 applies only to the flow just downstream of the normal portion of the wing leading-edge shock wave. Proceeding outboard, the wing leading-edge shock wave weakens rapidly, so that the flow downstream of the shock is again supersonic. The supersonic flow which exists downstream of the wing leading-edge shock outboard of the interaction region has a significant influence on the flowfield, as will be discussed subsequently. The current theoretical flow model assumes the local Mach number and, therefore, the static pressure to be constant in Region 7, i.e., the region adjacent to the wall and downstream of the Mach reflection. However, the varying strength of the wing leading-edge shock noted previously affects the flow in Region 7, as will be discussed.

The experimental pressure distribution along the plane of symmetry is compared in Fig. 5 with the theoretical values computed using the numerical code. As noted previously, the numerical code does not calculate the shock-interaction location without some empirical information. For the calculations presented in Fig. 5, the impingement point for the theoretical pressure distribution was determined from the schlieren photograph. Therefore, the location of the measured shock-induced pressure rise is the same as the location of the "theoretical" interface between Region 3 and Region 7. As noted previously, the current flow model assumes that the static wall-pressure is constant downstream of the impingement point, i.e., in Region 7. However, the shock-induced pressure rise does not approach the theoretically predicted jump, and it is measured at only a few orifices. Since the experimental pressure distribution represents measurements from a finite number of orifices, it is possible to miss the maximum value. Nevertheless, the pressure data are believed to reflect the true character of the shock-interaction structure. The pressure decreases significantly downstream of the impingement, asymptotically approaching a constant value.

To understand the measured pressure distribution, consider the pressure immediately downstream of the wing shock. The wing shock (see Fig. 4) may be divided into 3 segments: 1) that which divides Region 2 from Region 3 (or the "wing-root" shock); 2) that which divides Region 2 from Region 5; and 3) that which divides Region 1 from Region 6 (or the "wing-leading-edge" shock). The pressure immediately downstream of the shock was calculated using the schlieren trace of the shock wave and the theoretical Mach number just upstream of the shock-wave elements. The pressure distribution, thus calculated, is compared with the data from the plane of symmetry. The surface pressure measurements from Region 3 are lower than the value computed using the numerical routine but essentially equal to calculated pressure behind the experimentally observed shock wave. The differences between the computed solution and the data have been discussed previously.A sharp increase is evident in the pressure just downstream of the shock which divides Region 2 from Region 5. Recall that the pressure in Region 4 (just downstream of the impinging shock) is equal to the pressure in Region 5. Thus, one would expect the pressure in Region 7 (i.e., at the surface just downstream of the reflection) would be even higher. However, the pressure perturbation indicated by these calculations based on the schlieren photograph was not measured, perhaps because of the limited number of orifices of finite size, as noted previously. Outboard of the interaction region (i.e., for $s>0.5L$), the pressure just downstream of the wing leading-edge shock wave correlated closely with the pressures measured at the wedge surface. The agreement should be expected since the pressure gradient normal to the surface would be small in the absence of significant survature of the streamlines. The correlation of the experimentally determined static wall-pressure distribution with the pressure distribution just downstream of the wing leading-edge shock indicates that the flow model presently used in the theoretical code[8] is not adequate for the region downstream of the shock impingement (since the constant theoretical value for Region 7 is much higher than either the data or the values based on the shock shape).

The Type-VI Results

The schlieren photograph of the flowfield for $\delta=15°$ and $\Lambda=49.5°$, which is presented in Fig. 6, indicates that the shock interaction is a Type-VI pattern. The experimentally-determined flowfield is compared with the theoretical solution (the broken lines in Fig. 6). Clearly evident in the photograph are: the impinging "bow" shock wave, the linear shock wave dividing Region 2 from Region 3 (i.e., the "wing-root" shock wave), the centered expansion fan (i.e., Region 4), the "wing leading-edge" shock wave, which divides the freestream flow (Region 1) from the flow in Region 6, and the shear layer which is approximately parallel to the second wedge and which divides the flow which has passed through 2 shock waves from the flow which has passed through only 1 shock wave (i.e., the wing leading-edge shock). The "bow" shock wave is curved (reflecting three-dimensional effects) and, therefore, intersects the wing-root shock wave inboard of the theoretical solution. Also evident in the schlieren photograph are 2 weak (Mach) waves which occur when the flow on the second wedge is perturbed by the transverse rows of static orifices. Both perturbations occur in Region 3. Thus, an experimental value for the local Mach number in Region 3 was calculated using the measured wave angles, since $M=1/\sin\mu$.

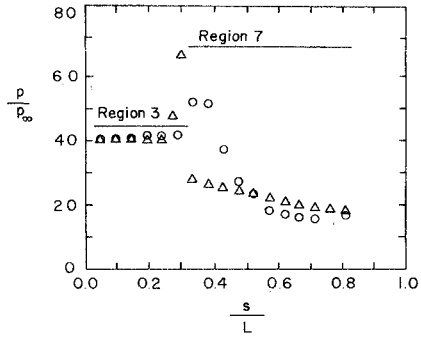

Fig. 5 Comparison of the experimental static pressure distribution along the second wedge with the values immediately downstream of the shock and with the theoretical values: $M_\infty=4.97$, $\delta=15°$, $\Lambda=41°$. —— Theory (code of Ref. 8); Δ Pressure immediately behind the shock determined using the shock-wave-angle distribution in the schlieren photograph (Fig. 4); o Static pressure measured on the surface of the second wedge.

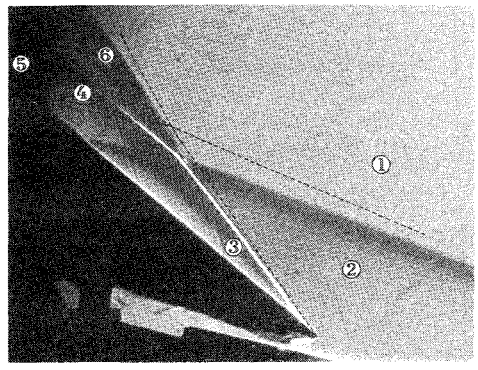

Fig. 6 Comparison of the theoretical flowfield using the Type-VI code of Ref. 7 with the schlieren photograph: $M_\infty=4.97$, $\delta=15°$, $\Lambda=49.5°$. Theoretical Mach numbers: Region 1: 4.97, Region 2: 3.49, Region 3: 1.95, Region 4: 2.02, Region 5: 2.11, Region 6: 1.15.

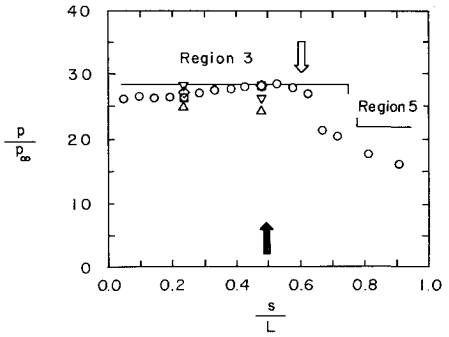

Fig. 7 Comparison of the experimental static pressure distribution along second wedge with the theoretical values: $M_\infty = 4.97$, $\delta = 15°$, $\Lambda = 49.5°$. —— Theory (code of Ref. 7); ⇐ Interaction region as determined from the schlieren photograph; ← Intersection of Mach waves from corners; Pressure data: y/L ○ 0.0000, ◇ 0.0597, □ 0.1194, ▽ 0.1791, △ 0.2388.

Experimentally, the local Mach number is 1.9 which is equal (to the nearest tenth) to the theoretical value.

The pressure measurements for the second wedge, i.e., the simulated wing leading edge, are presented in Fig. 7. Also included is the theoretical pressure distribution, as calculated using the numerical code described in Ref. 7. The pressure measurements from the plane of symmetry are in good agreement with the theoretical values in Region 3. Note that the location where the expansion fan impinges on the sufrace as determined using the pressure distribution agrees with that determined using the schlieren photograph (which is indicated in Fig. 7 by an arrow) but is inboard of the theoretical location. The difference between the theoretical and the experimental locations is approximately 0.8 cm. (0.3 in.). The intersection of the Mach waves emanating from the corner (the solid arrow of Fig. 7) is shown to indicate the limit of the two-dimensional flow in the plane of symmetry. The intersection occurs downstream of the two stations at which orifices were located off the plane of symmetry. At $s = 0.24$L, the pressure variation in the transverse, or y, direction is 7% of the static pressure measured in the plane of symmetry. At $s = 0.48$L, the transverse pressure variation is 13%. Downstream of the interaction-perturbed region, i.e., in Region 5, the experimental pressures are somewhat below theory. The difference is attributed to three-dimensional effects. However, based on the experimental transverse pressure gradients, it is concluded that the three-dimensional effects do not affect the character of the flow.

Conclusions

Over the range of geometries tested in the present program, the following conclusions are made: 1) Whereas theoretical solutions both for a Type-V pattern and for a Type-VI pattern can be generated for a particular test condition (as defined by the geometry and the freestream conditions), the weaker shock pattern was observed experimentally.

2) That portion of the second wedge which was affected by the shock-interaction moved inboard as the sweep angle decreases. The location of the interaction-perturbed region was a continuous function of sweep angle even as the interaction changed character.

3) The correlation between the measured Type-V shock-interaction pattern and the theoretical solution was satisfactory up to the region where the interaction intersected the surface. The Type-V pattern varied with sweep angle as was predicted by the theoretical model. The pressure distribution along the second wedge differed significantly from the calculated distribution. The weakening of the leading-edge shock wave outboard of the interaction had a marked effect on the surface pressure.

4) There was satisfactory agreement between the experimentally observed Type-VI shock-interaction pattern and the theoretical solution.

References

[1] Edney, B., "Anomalous Heat Transfer and Pressure Distributions on Blunt Bodies at Hypersonic Speeds in the Presence of an Impinging Shock," Rept. 115, 1968, Flygteckniska Forsoksanstalten (The Aeronautical Research Institute of Sweden), Stockholm.

[2] Hains, F.D. and Keyes, J.W., "Shock Interference Heating in Hypersonic Flows," *AIAA Journal*, Vol. 10, Nov. 1972, pp. 1441-1447.

[3] Bertin, J.J., Graumann, B.W., and Goodrich, W.D., "Aerothermodynamic Aspects of Shock-Interference Patterns for Shuttle Configurations During Entry," AIAA Paper 73-238, Washington, D.C., 1973.

[4] Hunt, J.L. and Creel, T.R., Jr., "Shock-Interference Heating and Density-Ratio Effects, Pt. II: Hypersonic Density-Ratio Effects," *NASA Space Shuttle Technology Conference, Vol. I:Aerothermodynamics, Configurations, and Flight Mechanics*, TMX-2272, April 1971, NASA.

[5] Bertin, J.J., Graumann, B.W., and Goodrich, W.D., "Analysis of High Velocity and Real-Gas Effects on the Shock-Interference Pattern for Delta-Wing Orbiters," AIAA Paper 74-522, Palo Alto, Calif., 1974.

[6] Ames Research Staff, "Equations, Tables, and Charts for Compressible Flow," Rept. 1135, 1953, NACA.

[7] Bertin, J.J. and Graumann, B.W., "Analysis of a Two-Dimensional Type VI Shock-Interference Pattern Using a Perfect-Gas Code and a Real-Gas Code," Aerospace Engineering Rept. 73003, Aug. 1973, The University of Texas at Austin, Austin, Texas.

[8] Graumann, B.W., "Theoretical Analysis of Shock: Shock Interaction Patterns for Two-Dimensional Flows," M.S. thesis, Jan. 1974, Department of Aerospace Engineering and Engineering Mechanics, The University of Texas at Austin, Austin, Texas.